Protein Transduction Domains of HIV-1 and SIV TAT Interact with Charged Lipid Vesicles. Binding Mechanism and Thermodynamic Analysis†

André Ziegler, Xiaochun Li Blatter, Anna Seelig, and Joachim Seelig*

Department of Biophysical Chemistry, Biozentrum, University of Basel, Klingelbergstrasse 70, CH-4056 Basel, Switzerland

Received April 29, 2003; Revised Manuscript Received June 12, 2003

ABSTRACT: Cell-penetrating peptides (CPPs) traverse cell membranes of cultured cells very efficiently by a mechanism not yet identified. Recent theories for the translocation suggest either the binding of the CPPs to extracellular glycosaminoglycans or the formation of inverted micelles with negatively charged lipids. In the present study, the binding of the protein transduction domains (PTD) of human (HIV-1) and simian immunodeficiency virus (SIV) TAT peptide (amino acid residues 47−57, electric charge $z_p = +8$) to membranes containing various proportions of negatively charged lipid (POPG) is characterized. Monolayer expansion measurements demonstrate that TAT-PTD insertion between lipids requires loosely packed monolayer films. For densely packed monolayers ($\pi > 29$ mN/m) and lipid bilayers, no insertion is possible, and binding occurs via electrostatic adsorption to the membrane surface. Light scattering experiments show an aggregation of anionic lipid vesicles when the electric surface charge is neutralized by TAT-PTD, the observed stoichiometry being close to the theoretical value of 1:8. Membrane binding was quantitated with isothermal titration calorimetry and three further methods. The reaction enthalpy is $\Delta H° \approx -1.5$ kcal/mol peptide and is almost temperature-independent with $\Delta C_p° \sim 0$ kcal/(mol K), indicating equal contributions of polar and hydrophobic interactions to the reaction heat capacity. The binding of TAT-PTD to the anionic membrane is described by an electrostatic attraction/chemical partition model. The electrostatic attraction energy, calculated with the Gouy−Chapman theory, accounts for ∼80% of the binding energy. The overall binding constant, K_{app}, is $\sim 10^3-10^4$ M^{-1}. The intrinsic binding constant (K_p), corrected for electrostatic effects and describing the partitioning of the peptide between the lipid−water interface and the membrane, is small and is $K_p \sim 1-10$ M^{-1}. Deuterium and phosphorus-31 nuclear magnetic resonance demonstrate that the lipid bilayer remains intact upon TAT-PTD binding. The NMR data provide no evidence for nonbilayer structures and also not for domain formation. This is further supported by the absence of dye efflux from single-walled lipid vesicles. The electrostatic interaction between TAT-PTD and anionic phosphatidylglycerol is strong enough to induce a change in the headgroup conformation of the anionic lipid, indicating a short-lived but distinct correlation between the TAT-PTD and the anionic lipids on the membrane outside. TAT-PTD has a much lower affinity for lipid membranes than for glycosaminoglycans, making the latter interaction a more probable pathway for CPP binding to biological membranes.

Cell-penetrating peptides (CPPs)[1] are a group of highly charged (Lys- and Arg-rich) peptides that traverse biological membranes within minutes (for a review, see ref *1*). CPPs are of quite diverse molecular origin and comprise, for example, the trans-acting activator of transduction (TAT) from HIV-1 and SIV (*2*, *3*), penetratin (pAntp) from *Drosophila*, vp22 from herpes simplex virus, and transportan, a synthetic compound. CPPs are potentially interesting for nonviral gene transfer, for drug administration, and for the understanding of cell transport mechanisms in general because they may act as a key to open the biological membrane for a multitude of covalently bound compounds that would not cross the membrane otherwise (*1*).

The physical mechanism of the rapid and efficient membrane translocation is not yet identified. Common to all CPPs is a highly charged cationic domain that is essential for transport. On the other hand, it is common knowledge that charged molecules cannot cross the lipid bilayer by passive diffusion because of the high Born charging energy encountered in a medium of low dielectricity. Nature has developed special transport systems such as ion carriers, channels, and ATP-coupled pumps to regulate the ion flow across biological membranes. From a physical-chemical point of view, it is hence surprising that short peptides containing a high percentage of cationic amino acids can nevertheless cross the plasma membrane of living cells by a seemingly energy-independent pathway. Moreover, these cell-penetrating peptides can be conjugated with larger biomolecules and

† This work was supported by the Swiss National Science Foundation Grant 31-58800.99

* To whom correspondence should be addressed. Tel: +41-61-267 2190. Fax: +41-61-267 2189. E-mail: joachim.seelig@unibas.ch.

[1] Abbreviations: CD, circular dichroism; CPPs, cell-penetrating peptides; HIV, human immunodeficiency virus; ITC, isothermal titration calorimetry; LUVs, large unilamellar vesicles, diameter ∼50 or 100 nm; POPC, 1-palmitoyl-2-oleoyl-*sn*-glycero-3-phosphocholine; POPG, 1-palmitoyl-2-oleoyl-*sn*-glycero-3-phospho-*rac*-glycerol; PTD, protein transduction domain; SIV, simian immunodeficiency virus; SUVs, small unilamellar vesicles, diameter ∼30 nm; TAT, trans-acting activator of transcription; TAR, TAT activation region.

10.1021/bi0346805 CCC: $25.00
Published on Web 07/10/2003

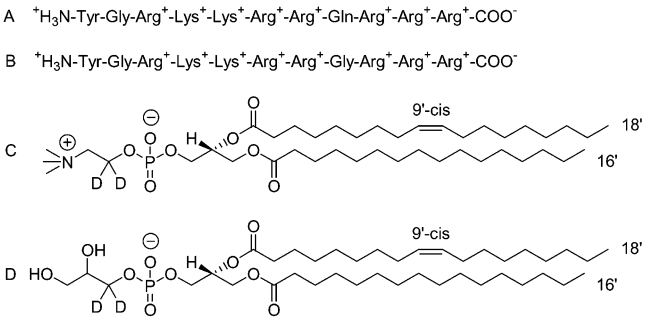

FIGURE 1: Chemical structure (A) HIV-1 TAT-PTD, (B) SIV TAT-PTD, (C) POPC = 1-palmitoyl-2-oleoyl-*sn*-glycero-3-phosphocholine deuterated at the α-segment of the choline headgroup segment, and (D) POPG = 1-palmitoyl-2-oleoyl-*sn*-glycero-3-phospho-*rac*-glycerol deuterated at the α-segment of the glycerol headgroup moiety.

can successfully cargo macromolecules and supramolecular entities such as nanoparticles into the cell interior.

It is currently not clear whether CPP translocation can be reproduced with simple membrane model systems composed of lipids only. The few available results are controversial. In one study, pAntp was claimed to be taken up into giant vesicles (*4*), whereas in another study pAntp did not traverse the membrane of small vesicles (*5*).

Two mechanisms are proposed at present as to how charged peptides could cross the hydrophobic barrier of a biological membrane without utilizing an active transport system. One possibility is complex formation of the cationic peptide with heparan sulfate proteoglycans to form an electrically neutral complex with consecutive adsorptive endocytosis (*2*, *6*). An alternative mechanism invokes the binding of CPPs to negatively charged lipids and the disruption of the bilayer structure via the formation of inverted micelles (*7*, *8*).

Using a variety of physical-chemical techniques, we have therefore investigated systematically the interaction of a specific CPP, the TAT protein transduction domain (TAT-PTD) of HIV-1 and SIV, with membranes containing various percentages of anionic lipid. Monolayer insertion studies provide an estimate of the average peptide insertion area. The thermodynamic binding parameters and the binding mechanisms were deduced with light scattering, monolayer expansion measurements, high sensitivity isothermal titration calorimetry (ITC), ζ-potential measurements, and ultracentrifugtion of sucrose-loaded vesicles. Deuterium (^{2}H) and phosphorus (^{31}P) NMR in combination with selectively deuterated lipid determined the structure of the lipid phase with and without peptide and were corroborated by dye-efflux measurements. Finally, the TAT-PTD binding to lipid membranes is compared to TAT-PTD interaction with glycosaminoglycans.

EXPERIMENTAL PROCEDURES

Materials. 1-Palmitoyl-2-oleoyl-*sn*-glycero-3-phospho-*rac*-glycerol (POPG), sodium salt, and 1-palmitoyl-2-oleoyl-*sn*-glycero-3-phosphocholine (POPC) were obtained from Avanti Polar Lipids Inc. (Alabaster, AL). For solid-state NMR measurements, POPC and POPG were deuterated at the headgroup moiety (i.e., at the α-carbon of the choline and the glycerol residue, respectively) (Figure 1). The synthesis of the deuterated lipids has been described previously (*9*, *10*). *N*-α-Fmoc-protected amino acids and OH-functionalized acid-labile TGA resin were purchased from Novabiochem (Laufelfingen, Switzerland).

Synthesis and Purification of TAT-PTD. The two peptides employed in this study are shown in Figure 1. They differ in the amino acid at a single position that is either Gly or Gln. Peptide I represents amino acids 47−57 of the human immunodeficiency virus HIV-1 TAT protein, which is a 86 (or 102) amino acid polypeptide. Peptide II is the corresponding domain of the simian immunodeficiency virus (SIV) TAT peptide. If not specified otherwise, the human TAT-PTD is used in the experimental studies. Both peptides contain six Arg and two Lys residues and are thus highly charged (net charge $z_p = +8$ at physiological pH). Solid-phase peptide synthesis of the 11-amino acid HIV-1 TAT-PTD (H_3N^+-YGRKKRRQRRR-COO^-, MW 1560.81) was performed on an Abimed EPS221 peptide synthesizer (Langenfeld, Germany) using Fmoc protected amino acids. After synthesis, the peptide was purified by preparative high-pressure liquid chromatography (HPLC) on a reverse phase column Lichrosorb RP-18/250-25 (Merck, Darmstadt, Germany) using a flow rate of 15 mL/min at 70 bar and a linear elution gradient from 5 to 10% acetonitrile within 1 h. The mass of the peptide was confirmed by electrospray ionization mass spectrometry (Finnigan TSQ7000; San Jose, CA). Peptide purity (>98%) was measured by analytical HPLC. After purification, the peptide was suspended in water, neutralized to pH 7.40, and lyophilized. The effective peptide concentration was measured as amino acid content after acid hydrolysis. The SIV TAT-PTD with sequence H_3N^+-YGRKKRRGRRR-COO^- was purchased from SynPep (Dublin, CA).

Buffer. Solutions were prepared with buffer containing either 100 mM NaCl, 10 mM TRIS-HCl, pH 7.4 (monolayer measurements, dye release, microelectrophoresis, ITC) or 70 mM NaCl, 30 mM phosphate, pH 7.4 (some ITC measurements). The samples were filtered (0.44 μm) and degassed immediately before use (140 mbar, 8 min). For sucrose-loaded vesicles, MOPS instead of TRIS was used since fluorescamine reacts with primary amines (*11*).

Preparation of Lipid Vesicles. POPG was dried from a stock solution in chloroform by a gentle stream of nitrogen followed by vacuum (0.2 mbar) overnight. The amount of POPG was weighed, and a defined volume of a POPC stock solution in chloroform was added to yield the desired POPG/POPC molar ratio. The solvent was evaporated by a continuous stream of nitrogen leading to a thin lipid film, which was dried under vacuum overnight and weighed again. Buffer was added to the dry lipid film leading to a final lipid concentration of 20−40 mM. After flushing with argon, the lipid dispersion was vortexed, leading to multilamellar vesicles (MLVs). The MLVs were transformed to unilamellar vesicles of defined size either by sonication or nanopore filtration. Small unilamellar vesicles (SUVs) with an average diameter of 30 nm were prepared by sonication (Branson Sonifier, Danbury, CT; 50 W/mL) for 30 min under a nitrogen atmosphere (at 4 °C) until an almost clear solution was obtained. Metal debris from the sonicator tip was removed by centrifugation at 16 000*g* for 10 min. Large unilamellar vesicles (LUVs) with a diameter of 50 or 100 nm were produced by subjecting the MLVs to five consecutive freeze−thaw cycles and subsequent extrusion through

polycarbonate filters with 50 or 100 nm pore size (Whatman, Clifton, NJ) using a hand extruder (Avanti, Alabaster, AL).

Monolayer Measurements. Monolayer experiments were performed as described previously (*12*). The surface activity was measured in a 3 mL home-built trough. Insertion experiments were made in one compartment of a round Teflon trough (type RCM 2-t, Mayer Feintechnik, Göttingen, Germany) with a surface area of 45.25 cm^2 and a volume of 20 mL. The trough was covered by a Plexiglas hood to keep humidity constant. The surface pressure, $\pi = \gamma_0 - \gamma$, where γ_0 is the surface tension of the pure buffer and γ is the surface tension of the peptide solution, was monitored by means of Whatman no. 1 filter paper, connected to a Wilhelmy balance. Measurements were performed at 21 ± 1 °C.

For insertion experiments, a monolayer was formed by depositing a drop of lipid dissolved in hexane/ethanol (9:1, v/v) on the buffer surface between a fixed and a movable barrier and was then left to stabilize for about 15 min. The initial area, A (typically around 40 cm^2), contained n_L lipid molecules of an area A_L. Protein (~1 mg/mL) dissolved in water was injected into the buffer subphase and was left to equilibrate between the aqueous and the lipid phase. The surface pressure, π, was kept constant during the insertion experiments by means of an electronic feedback system. The insertion of n_P protein molecules with an insertion area of A_P into the monolayer thus gave rise to an area expansion, ΔA. The mole fraction of protein in the monolayer is defined as $X_b = n_P/n_L$ and can be evaluated from the relative area increase, $\Delta A/A$, provided A_L and A_P are known (*13*)

$$X_b = n_P/n_L = (\Delta A/A)(A_L/A_P) \quad (1)$$

As a first approximation, the binding to the lipid membrane can be described in terms of a simple partition equilibrium

$$X_b = K_{app} C_{eq} \quad (2)$$

where K_{app} is the apparent binding constant (see ref *14*).

To penetrate into a lipid monolayer with a lateral pressure π, a protein molecule has to perform the work, $\Delta W = \pi A_P$, where the penetration area, A_P, is the area that the protein occupies in the lipid monolayer. The free energy of penetration will therefore vary with the monolayer surface pressure, π. According to Boguslavsky et al. (*15*), the variation of the binding constant with pressure is given by

$$K = K_0 e^{-\pi A_P/kT} \quad (3)$$

Combining eqs 1 and 3 yields the surface pressure dependence of the relative area increase, $\Delta A/A$, at constant C_{eq} under the assumption of a constant penetration area, A_P, and a constant lipid area, A_L.

$$\Delta A/A = (A_P/A_L) K_0 C_{eq} e^{-\pi A_P/kT} \approx \text{constant } e^{-\pi A_P/kT} \quad (4)$$

The measured pressure dependence of the $\Delta A/A$ curves can then be used to determine the penetration area, A_P. A lipid cross sectional area of $A_L = 0.68$ nm^2 was assumed in all calculations.

Isothermal Titration Calorimetry. The heat flow resulting from the binding of the TAT-PTD peptides to lipid vesicles was measured by high-sensitivity isothermal titration calorimetry using a Microcal VP-ITC calorimeter (Microcal, Northampton, MA) with a reaction cell volume of 1.4037 mL. Typical peptide concentrations were ~30 μM. Most experiments were performed with vesicles containing 25% negatively charged POPG. Peptide concentrations >30 μM were usually avoided to prevent baseline drifts caused by aggregate formation. At 50% POPG content peptide concentrations of up to 80 μM could be used. Binding isotherms were measured by lipid-into-peptide titrations (*4*). The peptide solution was filled into the calorimeter cell, and lipid vesicles were injected through a syringe. The injection volumes were 5−10 μL. Solutions were degassed immediately before use (140 mbar, 8 min).

Leakage Experiments. Calcein-loaded POPC/POPG (75:25) vesicles were prepared as described previously (*16*). The tat-induced leakage of calcein from the vesicles was monitored by measuring the increase in fluorescence intensity at 520 nm (excitation at 490 nm) on a Jasco FP 777 fluorimeter (Tokyo, Japan) at 25 °C. The fluorescence intensity corresponding to 100% calcein release was determined by the addition of 100 μL of 10% Triton-X solution.

NMR Spectroscopy. All spectra were acquired at a magnetic field strength of 9.4 T. For the ^{2}H-NMR measurements, a quadrupole echo sequence was employed using a recycle delay of 250 ms. ^{31}P-NMR spectra were recorded a using a Hahn echo sequence with broadband proton decoupling (WALTZ-16) and a recycle delay of 6 s. The chemical shielding anisotropy, $\Delta\sigma$, was measured as full width at 10% maximum intensity. Samples were prepared using typically 40 mg of total lipids and 150−200 μL of deuterium-depleted water. The peptide was added before vortexing the lipid film.

RESULTS

Surface Activity and Monolayer Penetration Studies. For HIV-1 TAT-PTD and SIV TAT-PTD an initial rise in surface pressure is observed at a concentration of 5 μM. At a peptide concentration of 25 μM, the surface pressure is 2.5 mN/m. Evaluation of the Gibbs adsorption isotherm in the concentration range of 5 μM < C < 25 μM yields a surface area requirement of the peptide of $A_S = 2.5$ nm^2. For comparison, a peptide area of ~7 nm^2 was estimated from a molecular model with the peptide lying flat on the air−water interface.

Using lipid monolayers kept at constant lateral pressure by an electronic feedback system we have investigated the tendency of HIV-1 and SIV TAT-PTD peptide to insert between the lipid molecules. Insertion is detected by an area increase of the monolayer. Figure 2 displays the relative area increase, $\Delta A/A$ as a function of the lateral pressure π. The peptide concentration in the subphase was chosen as $C_{pep} = 1.54$ μM. For mixed POPC/POPG (75:25 mol %) monolayers, insertion of TAT-PTD peptide takes place up to a lipid packing density of 28 mN/m. At higher lateral pressure, the insertion was too small to be detected. The insertion area of both TAT-PTDs was estimated by the procedure outlined above as $A_p \approx 0.95-1.0$ nm^2, which is larger than the cross-sectional area of a single lipid molecule, $A_L = 0.68$ nm, but distinctly smaller than the surface area requirement of the peptide with $A_S = 2.5$ nm^2. Only a fraction of the peptide surface can insert between the lipids of a loosely packed monolayer. More importantly, the peptide cannot be expected to penetrate into a lipid bilayer since the latter is characterized by a monolayer equivalence pressure of >32 mN/m (*13*).

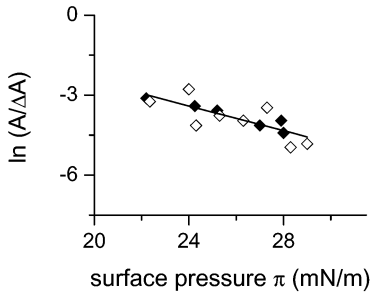

FIGURE 2: Insertion of HIV-1 TAT-PTD (◇) and SIV-TAT-PTD (◆) into a lipid monolayer composed of POPC/POPG (3:1 mol/mol). The lipid monolayer is kept at a preset lateral pressure, π, and the peptide is injected into the subphase (10 mM TRIS-HCl, 100 mM NaCl, pH 7.4) with a final concentration of $C_{p,tot} = 1.57$ μM. The relative change in area, $\Delta A/A$, is plotted as a function of lateral pressure.

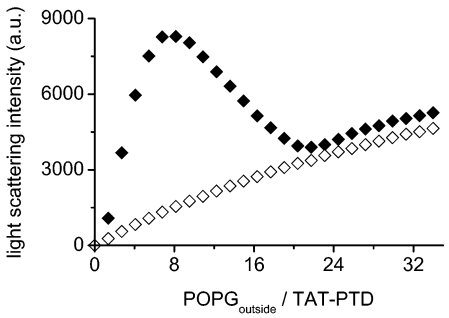

FIGURE 3: Static right-angle light scattering. Titration of lipid vesicles into a TAT-PTD solution. The concentration of TAT-PTD in the optical cuvette is 8 μM ($V_{cell} = 2.8$ mL). Each data point corresponds to the injection of 20 μL (every minute) of sonicated (30 nm) lipid vesicles. The lipid composition is POPC/POPG 3:1 mol/mol. The total lipid concentration in the injection syringe is 10 mM; hence, the POPG concentration is 2.5 mM. The solid symbols represent the change in light-scattering as a function of the $POPG_{outside}$/TAT-PTD ratio. Only the lipid in the outer monolayer (60% = 1.5 mM) was assumed to be available for binding. The open symbols are the control obtained by injecting the same lipid suspension into pure buffer only. Buffer composition 10 mM TRIS-HCl, 100 mM NaCl, pH 7.4. Temperature 28 °C.

With an insertion area of $A_p = 1.0$ nm^2, an apparent binding constant $K_{app} = 3.2 \times 10^3$ M^{-1} was obtained.

Light Scattering. Small unilamellar vesicles composed of POPC/POPG (75:25 mol %) were mixed with a clear solution of TAT-PTD and immediately produced a marked increase in turbidity. Upon addition of more lipid vesicles, the scattering intensity decreased again. The solution remained, however, turbid because of the intrinsic scattering of the lipid vesicles.

The aggregation process was analyzed quantitatively with right-angle light scattering. The titration of TAT-PTD peptide with 30 nm lipid vesicles composed of POPC/POPG (75:25 mol %) is shown in Figure 3. The scattering intensity is plotted as a function of the lipid/TAT-PTD ratio. It increases smoothly until a maximum is reached at about 7.6 ± 0.5 POPG per TAT-PTD (mean ± SD, $n = 4$). This result is calculated with the assumptions that (i) sonicated 30 nm vesicles have 60% of their total lipid on the outside and (ii) only the anionic POPG on the lipid outside is available for peptide binding. As more lipid is added the scattering intensity decreases again, indicating a reversal of the aggregation process. The reduction in light scattering intensity is not caused by a dilution effect since each data point corresponds to the addition of only 20 μL of lipid suspension into a total volume of 2.8 mL. The remaining scattering intensity at high lipid-to-peptide ratios can be explained by the intrinsic scattering of the lipid vesicles. This can be visualized by a vesicle-into-buffer titration in the absence of TAT-PTD (Figure 3, open symbols).

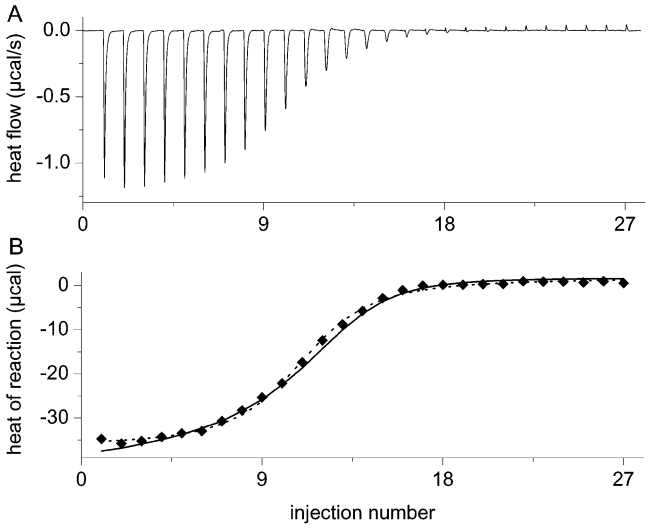

FIGURE 4: Isothermal titration calorimetry. Titration of sonicated lipid vesicles into a SIV TAT-PTD solution. (A) Heat flow: the reaction cell has a volume of $V_{cell} = 1.4037$ mL and contains the TAT-PTD peptide at a concentration of 61.7 μM. Each peak corresponds to a 5 μL injection of 30 nm POPC/POPG (1:1) vesicles at a total lipid concentration of 37.5 mM (in buffer). (B) Heats of reaction (integration of the heat flow peaks in panel A) as a function of the injection number. The dashed line corresponds to the complex formation model, and the solid line is the electrostatic attraction/chemical partition model (cf. Table 1 for parameters).

Isothermal Titration Calorimetry and Multi-Site Binding Model. Titration of TAT-PTD with POPC/POPG vesicles gives rise to exothermic titration patterns. Figure 4A displays the result obtained for 30 nm vesicles of high POPG content (POPC/POPG 50:50 mol %). The peptide (SIV TAT-PTD) is contained in the calorimeter cell, and 30 nm POPC/POPG (1:1 mol/mol) vesicles in phosphate buffer are added in 5 μL aliquots. For the first four injections, an almost constant heat release is observed. As the titration continues, the free peptide concentration in the cell decreases, and the heat flow decreases in parallel. Figure 4B shows the heats of reaction, h_i, obtained by integration of the heat flow peaks. In the course of the titration, the free TAT-PTD concentration in the calorimeter cell decreases from 61.5 μM at the beginning of the titration to 0.1 μM after 20 lipid injections. Hence, the lipid-into-peptide titration leads to a complete binding of all peptide contained in the measuring cell. The molar binding enthalpy, ΔH°_{exp}, can thus be determined directly from the cumulative heat release and independent of any particular binding model (cf. Table 1).

The plateau region in Figure 4 indicates that the same amount of peptide binds to the lipid vesicles in each of the first four injections. Comparing the individual heat release (−37 μcal) with the total (cumulative) heat release (−395 μcal) reveals that approximately 1/10 of the total amount of peptide in the calorimeter cell is bound in a single injection of lipid. During the initial phase of the titration, the added POPG appears to be saturated with TAT-PTD since the peptide is much in excess over the POPG lipid. An empirical

Table 1: Parameters for TAT-PTD Binding to Unilamellar Phospholipid Vesicles of Different Size and Content of Anionic POPG

					complex formation model			electrostatic attraction/ chemical partition model				
T (°C)	vesicle size (nm)	nominal PG content of total lipid (%)	fraction of total lipid in outer layer that is PG	$\Delta H_{exp}{}^0$ (kcal/mol)	number of lipids bound per TAT	$\Delta H_{complex}$ (kcal/mol)	K_0 (M^{-1})	peptide charge z_p	ΔH_{GCT} (kcal/mol)	K_p (M^{-1})	$\Delta G°$ (kcal/mol)	$T\Delta S°$ (kcal/mol)
100mM NaCl, 10mM Tris, pH 7.4												
Temperature[a]												
8	30	25	0.25	−1.5	7.9	−1.8	1.80E+04	3.2	−1.7	15	−1.51	−0.19
8								4.0	−1.7	8	−1.16	−0.54
18	30	25	0.25	−1.7	8.0	−1.8	1.50E+04	4.0	−1.8	8	−1.20	−0.60
28	30	25	0.25	−1.9	8.3	−1.6	1.30E+04	4.0	−2.0	7	−1.16	−0.88
28	30	25	0.25	−1.8	8.3	−1.8	1.20E+04	4.0	−1.7	7	−1.16	−0.55
38	30	25	0.25	−1.8	7.8	−1.9	1.10E+04	4.0	−1.8	6	−1.10	−0.70
48	30	25	0.25	−2.1	8.5	−2.0	9.00E+03	4.0	−2.0	5	−1.02	−0.98
Vesicle size[a]												
28	100	25	0.25	−0.9	8.0	−0.67	6.00E+04	7.0	−0.63	6	−1.07	0.44
28	100	25	0.25	−0.7	8.0	−0.7	7.00E+04	7.0	−0.67	4	−0.83	0.16
28	50	25	0.25	−1.6	8.0	−1.4	4.00E+04	6.0	−1.37	1.5	−0.24	−1.13
28	30	25	0.25	−1.8	8.3	−1.8	1.20E+04	4.0	−1.71	7	−1.16	−0.55
PG content[b]												
25	30	25	0.25	−1.5	8.0	−2.2	8.00E+03	4.0	−1.96	7	−1.15	−0.81
25	30	25	0.25	−1.4	8.0	−1.7	1.00E+04	4.0	−1.62	7	−1.15	−0.47
25	30	29	0.29	−2.9	8.0	−3.5	1.00E+04	4.0	−3.00	7	−1.15	−1.85
25	30	35	0.55	−3.0	8.0	−3.0	3.20E+04	4.6	−2.70	0.8	0.13	−2.83
25	30	41	0.67	−3.1	8.0	−3.2	6.00E+04	6.0	−3.0	0.8	0.13	−3.13
25	30	50	0.67	−4.3	8.0	−4.6	1.10E+05	6.0	−4.5	1.2	−0.11	−4.39
25	30	50	0.67	−4.6	8.0	−4.6	1.10E+05	6.0	−4.5	1.2	−0.11	−4.39

[a] Measurement with (HIV-1) TAT-PTD. [b] Measurement with (SIV) TAT-PTD.

model to describe such an interaction is a multisite binding model in which the peptide carries n independent lipid binding sites. If $[M]_{total}$ is the total concentration of peptide (macromolecule) in the calorimeter cell, $[L]_{bound}$ the concentration of bound ligand (POPG lipid), and [L] the concentration of free ligand, then the equilibrium can be described by (*17*)

$$\frac{[L]_{bound}}{[M]_{total}} = n\frac{K_0[L]}{1 + K_0[L]} \quad (5)$$

$[L]_{bound}$ and [L] can be determined directly from the titration experiment together with the reaction enthalpy, $\Delta H°$ ($= \Delta H°_{exp}$) (*18*, *19*). It is then possible to evaluate n and K_0 according to the above equation. The dashed line in Figure 4B shows the application of this binding model resulting in the following set of parameters: $n = 8$, $K_0 = 1.1 \times 10^5$ M^{-1}, and $\Delta H° = -4.6$ kcal/mol. K_0 is the average binding constant of a single POPG binding to one of the TAT-PTD binding sites. K_0 is dependent on the PG content and is largest at 50% POPG. The stoichiometry of POPG/TAT-PTD = 8:1 is consistent with the lipid-to-peptide ratio observed at the maximum light scattering (Figure 2A). Despite the good agreement between experiment and theory, the multisite binding model is an empirical description in which important physical aspects are missing (cf. below).

The amount of POPG on the lipid vesicle outside and hence accessible for peptide binding can only be determined within certain limits. On the basis of geometric considerations, one expects about 60% (50%) of the total lipid in the outer layer if the vesicle has a diameter of 30 nm (100 nm). However, it has been shown by NMR shift reagents that for membranes with a high PG content, relatively more anionic lipid is on the outside than on the inside because of stronger and energetically unfavorable electrostatic headgroup interactions in the highly curved vesicle inside (*20*). For homogeneous PC/PG (50:50 mol %) vesicles with a diameter of 30 nm, it has been estimated that the outer surface of the bilayer vesicle contains twice as many PG as PC molecules (*20*). Under these conditions, not 60 but 80% of the total PG of the vesicle is located on the outer membrane leaflet. This effect was taken into account in evaluating Figure 4 and corresponding titrations. At low PG content (≤30% PG), a symmetric distribution of PG in both half-layers was assumed. For a PG content >30%, the PG fraction in the outer monolayer was preset at the result obtained by Michaelson et al. (*20*) assuming a POPG/POPC composition of 67:33 mol % in the outer monolayer and then slightly adjusting it to produce an optimal fit.

In a series of lipid-into-peptide ITC titrations, we have systematically varied (i) the POPG content, (ii) the temperature, and (iii) the vesicle size. At PG concentrations ≤35%, the plateau region seen in Figure 4A is no longer observed. Instead, the h_i values decrease in an approximately parabolic fashion. Again, an excellent fit of the calorimetric data was obtained with the multisite binding model using a POPG/TAT-PTD stoichiometry of $n = 8$. The parameters of the simulation are summarized in Table 1. Inspection of Table 1 allows the following conclusions. (i) The exothermic binding enthalpy, $\Delta H°$, grows linearly in magnitude with the POPG content of the membrane. This is paralleled by a distinct increase in the binding constant, K_0, and attests to a tight and enthalpy-driven lipid binding to TAT-PTD at high POPG contents. (ii) $\Delta H°$ varies with the vesicle size. $\Delta H°$ becomes less exothermic for large vesicles. (iii) For 30 nm vesicles with 25% POPG content, $\Delta H°$ is almost completely independent of temperature, and the molar heat capacity, $\Delta C_p°$, is close to zero ($\Delta C_p° = -13$ cal/mol K referred to TAT-PTD).

Isothermal Titration Calorimetry and Electrostatic Attraction/Chemical Partition Model. The multisite binding model is a chemical model that does not specifically consider the electrostatic interaction between POPG and TAT-PTD. An alternative description of the data is possible via the Gouy−Chapman theory by combining electrostatics with a chemical partition equilibrium. Since the lipid membrane is negatively charged, it has a negative surface potential Ψ_0. The cationic peptide is attracted to the membrane surface, and its concentration near the membrane, C_s, is considerably larger than the equilibrium concentration, C_{eq}, encountered at sufficient distance from the membrane. C_s can be calculated from C_{eq} by Boltzmann's law if Ψ_0 is known

$$C_s = C_{eq} e^{-z_p \Psi_0 F_0/RT} \quad (6)$$

Here, z_p is the effective peptide charge sensed at the membrane surface, F_0 is the Faraday constant, and RT is the thermal energy. The peptide partitions into the membrane, and the molar ratio of membrane-bound peptide, X_b, is assumed to be linearly proportional to the surface concentration C_s

$$X_b = K_p C_s \quad (7)$$

where K_p is the chemical (hydrophobic) partition coefficient (independent of electric effects). X_b is defined according to

$$X_b = \frac{n_{p,bound}}{n^0_{Lipid}} = \frac{C_{p,bound}}{C^0_{Lipid}} \quad (8)$$

where $n_{p,bound}$ and n^0_{Lipid} are the molar amounts of membrane-bound peptide and total accessible lipid (charged and neutral lipid), respectively; $C_{p,bound}$ and C^0_{Lipid} are the corresponding concentrations.

The surface potential, Ψ_0, can be derived by using the Gouy−Chapman theory (*21*, *22*). The combination of the Gouy−Chapman theory with a chemical equilibrium has proven to be a successful approach for a large variety of membrane equilibria. Different levels of sophistication are possible, and the specifics of our approach are given in detail in (*23*, *24*). The solid line in Figure 4B is the theoretical result. The experimental data are simulated with an effective peptide charge of $z_p = 6$ and a $K_p = 1.2\ M^{-1}$ leading to a good agreement between theory and experiment. A charge of $z_p = 6$ differs from the stoichiometric ratio of $n = 8$ deduced from the complex formation model. Apparently, not all charged residues of the TAT-PTD peptide reach the membrane surface simultaneously, be it for reasons of steric constraints within the peptide or be it for the strongly curved surface of the small unilamellar vesicles.

The Gouy−Chapman analysis is again based on a half-sided binding of TAT-PTD since we have no evidence that the highly charged peptide can cross the lipid bilayer. Only the POPG lipid of the outer monolayer enters into the calculation of Ψ_0. On the other hand, the total lipid content (POPC + POPG) of the outer monolayer is considered to act as a matrix for partitioning and is used to deduce the partition coefficient K_p.

The results of the electrostatic attraction/chemical partition model are included in Table 1. The partition constant, K_p, is 3 orders of magnitude smaller than the binding constant, K_0, determined for the multisite binding model. The difference is due to electrostatic attraction, and K_p represents only the remaining small hydrophobic interaction between TAT-PTD and membrane.

The electrostatic theory makes definite predictions about the variation of the membrane surface potential with the peptide concentration. These can be tested by measuring the electrophoretic mobility of lipid vesicles yielding, in turn, the so-called ζ-potential. The ζ-potential is the surface potential measured at a distance of about 0.2 nm away from the plane of peptide binding and can also be calculated with the Gouy−Chapman theory. We have measured the ζ-potential for multi-lamellar POPC/POPG (75:25 mol %) vesicles in the presence of various concentrations of TAT-PTD peptide. In buffer (100 mM NaCl, 10 mM Tris, pH 7.4), the ζ-potential of lipid vesicles without TAT-PTD is $\zeta = -37$ mV. It decreases rapidly to −24 mV at a TAT-PTD equilibrium concentration of 1 μM. The parameters derived from the ITC titration calorimetry correctly predict this variation of the ζ- potential. Since the ζ-potential measurements were made with large multilamellar vesicles, the parameters selected for the calculation corresponded to those derived for 100 nm vesicles.

A third method used to study peptide binding is to equilibrate sucrose loaded vesicles with peptide, to separate the vesicles from the solution by centrifugation, and to determine the remaining peptide concentration in the supernatant with a fluorescamine dye assay (*11*). The difference to the initial peptide concentration provides the amount of bound peptide. We employed this approach to POPC/POPG vesicles (75:25 mol %) and peptide (SIV TAT-PTD) concentrations of 1−10 μM. The data were analyzed in terms of the partition equilibrium described above but using bulk concentrations. This leads to an apparent (and concentration-dependent) binding constant K_{app} according to

$$X_b = K_{app} C_{eq} \quad (9)$$

where

$$K_{app} = K_p e^{-z_p \psi_0 F_0/RT} \quad (10)$$

K_{app} was found to decrease from $1 \times 10^4\ M^{-1}$ at 2 μM peptide concentration to $2.8 \times 10^3\ M^{-1}$ at 8 μM. This result is consistent with the ITC measurements. The electrostatic attraction/chemical partition model predicts K_{app} to decrease from 8×10^3 to $2.4 \times 10^3\ M^{-1}$ for the same concentration range (taking the parameters for 100 nm vesicles, cf. Table 1).

In summary, four independent methods (monolayer expansion, ITC, ζ-potential measurements, and equilibrium ultracentrifugation with sucrose-loaded vesicles) have been applied to measure the binding of TAT-PTD to negatively charged membranes. The data sets could be described with the electrostatic partition/chemical attraction model with the same set of parameters z_p and K_0, provided the Gouy−Chapman analysis was based on a half-sided binding of TAT-PTD to lipid vesicles.

Deuterium and Phosphorus-31 NMR of Lipid-TAT Interactions. Structural aspects of the TAT-PTD membrane interaction were investigated with solid-state nuclear magnetic resonance. Figure 5 shows the relevant NMR spectra

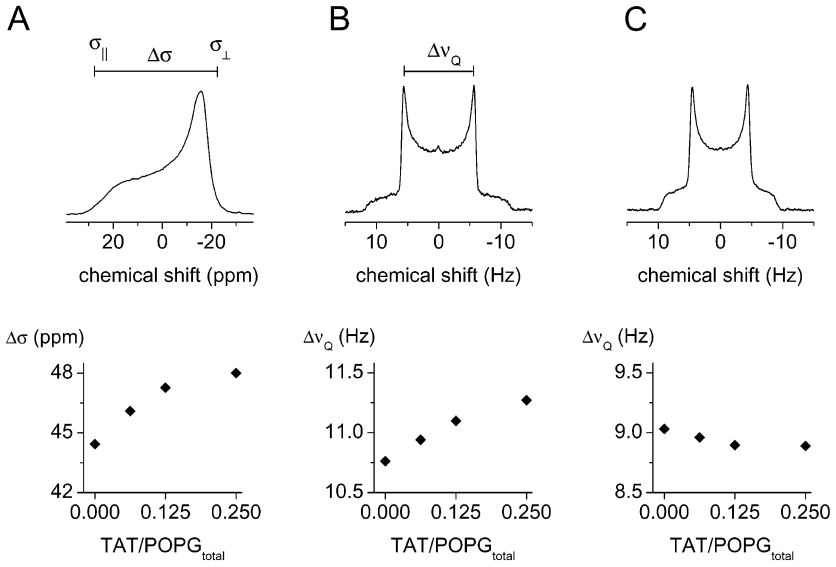

FIGURE 5: Deuterium and phosporus-31 NMR of multilamellar lipid dispersions containing various amounts of TAT-PTD. The top row shows typical phosphorus (A) and deuterium NMR (B and C) spectra in the presence of TAT-PTD. The membranes are composed of POPC/POPG (3:1 mol/mol), and the POPG:TAT-PTD ratio is 4:1 in all spectra. Panel A is the ^{31}P-NMR spectrum of the total lipid (POPC + POPG). Panel B shows the ^{2}H-NMR spectra of a POPC/POPG membrane in which the α-segment of POPG is selectively deuterated while POPC is not deuterated. (C) The POPC headgroup is deuterated at the α-segment while the POPG remains protonated. The bottom row shows the variation of the phosphorus chemical shielding anisotropy, $\Delta\sigma$, and the corresponding deuterium quadrupole splittings, $\Delta\nu_Q$, as a function of the TAT-PTD-to-POPG$_{total}$ ratio.

together with the evaluation of the characteristic spectral parameters. Phosphorus-NMR is highly sensitive to lipid polymorphism, and quite different spectra are obtained for planar lipid bilayers, hexagonal phases, and micellar structures (*25*). The phosphorus NMR spectrum shown in Figure 5A for POPG/POPC (25:75 mol %) dispersions in water provides unambiguous evidence for a homogeneous lipid bilayer at a molar POPG-to-TAT-PTD ratio of 4. The chemical shielding anisotropy (i.e., the separation between the edges of the ^{31}P-NMR spectra) increased by about 10% in the presence of TAT peptide indicating a small reorientation of the phospholipid headgroups.

This latter effect was investigated further with ^{2}H-NMR of mixed POPC/POPG membranes containing either POPG (Figure 5B) or POPC (Figure 5C) specifically deuterated at the lipid headgroup. The deuterated lipids were mixed with their nondeuterated counterpart to yield a POPC/POPG 75:25 molar ratio and were measured as multilamellar dispersions. All deuterium NMR spectra—with and without TAT-PTD peptide—were typical bilayer spectra with a single quadrupole splitting (Figure 5B,C upper panel). Under no conditions did we detect separate signals for free lipid and lipid complexed with TAT-PTD peptide. The lower panel in Figure 5 shows the variation of the phosphorus chemical shielding anisotropy, $\Delta\sigma$, and of the quadrupole splittings, $\Delta\nu_Q$, of the α-segments of the POPG and POPC headgroups (cf. Figure 1) as a function of the peptide-to-POPG ratio. The quadrupole splitting of the POPC headgroup is barely affected by the presence of TAT-PTD. In contrast, the quadrupole splitting of the POPG headgroup increases linearly with increasing TAT-PTD, indicating a preferential interaction of TAT-PTD with this negatively charged lipid.

DISCUSSION

The monolayer, ITC, NMR, and ζ-potential measurements provide clear evidence for the interaction of TAT-PTD peptide with the lipid membrane, provided the membrane carries a net negative charge. The binding process can be analyzed in two ways, namely (i) by a multisite binding model or (ii) by an electrostatic attraction/chemical partition model. The first approach assumes specific interactions between the PG lipids and the cationic peptide, with a finite number of lipid binding sites on the peptide. The second model is based on a nonspecific electrostatic accumulation of peptide near the membrane surface followed by a hydrophobic adsorption. The mathematical requirements are more elaborate for the latter approach, but the electrostatic attraction/chemical partition model is physically more realistic. In particular, the ζ-potential measurements can only be explained in terms of this model. In addition, if the temperature dependence of binding constants K_0 and K_P is analyzed via a van't Hoff plot, only the electrostatic attraction/chemical partition model (K_P) yields the $\Delta H°$ value derived with ITC.

The latter model is further supported by the NMR data described above. It has been demonstrated previously that the phosphocholine headgroup is sensitive to the electric charge at the membrane surface (*26*). In the electrically neutral state, the $^{-}$P−N^{+} dipole is approximately parallel to the membrane surface. When positively charged molecules bind, the $^{-}$P−N^{+} dipole moves with its N^{+} end toward the aqueous phase; negatively charged molecules induce the opposite movement toward the membrane interior. This reorientation is easily detected by a change in the deuterium quadrupole splitting of deuterated headgroup segments, and to a lesser extent, by a change in the phosphorus chemical shielding tensor (*27*). The observed reorientation is also quite independent of the chemical nature of the adsorbed species. It can be induced by such diverse agents as metal ions (*28*−*30*), local anesthetics (*31*, *32*), potential sensitive dyes (*33*), drugs (*34*, *35*), or peptides (*36*−*38*). The only exception from this general observation has been pentalysine. Roux et al.

(*39*) showed that Lys_5 binds strongly to mixed phosphatidylcholine/ phosphatidylserine (PS) membranes but has no effect on headgroup deuterated PC and only a small effect on headgroup deuterated PS. They suggested therefore that Lys_5 binds at some distance from the plane of the polar groups.

The electrostatic effects of polylysines have been investigated in more detail by Franzin and Macdonald (*40*). They demonstrated for mixed phosphatidylcholine/-serine membranes that domain formation can be induced with polylysines of a chain length of $n = 30$ or more but not with shorter peptides. These results are in agreement with a theoretical analysis of lipid demixing upon adsorption of charged proteins (*41*). Lipid domains are predicted to form when a highly charged protein binds to a weakly charged membrane at low levels of binding.

TAT-PTD carries more positive charges than Lys_5; nevertheless, its total charge is not sufficient to induce domain formation as evidenced by the present NMR measurements. At all temperatures and peptide concentrations investigated, a single quadrupole splitting was observed indicating a homogeneously mixed PC/PG lipid phase at this level of resolution and sensitivity. On the other hand, the ^{2}H-NMR reveals a small change in the orientation of the α-CH_2 segment of the POPG headgroup while that of the corresponding segment in POPC remains constant. This suggests a distinct positional correlation between TAT-PTD molecules at the membrane surface and the POPG headgroups. This correlation, although short-lived, is sufficient to change slightly the POPG headgroup conformation; however, it is not strong enough to induce phase separation.

The NMR spectra clearly document that the membrane remains intact as a stable lipid bilayer, at least up to a POPG-to-TAT-PTD ratio of 4. This is further supported by efflux experiments in which POPG/POPC (25:75 mol %) vesicles (100 nm diameter) were filled with a fluorescent dye (calcein). Addition of TAT-PTD induced no leakage (experiments not shown). It can be concluded that TAT-PTD binding to POPC/POPG bilayers does not induce the formation of leaky nonbilayer structures such as inverted micelles (*7*) or the hexagonal II phase, at least not at the present level of resolution.

Specific Aspects of the Gouy−Chapman Analysis. The Gouy−Chapman analysis leads to a partition coefficient, K_p, that describes exclusively the hydrophobic interaction between the peptide and the membrane. Table 1 demonstrates that K_p decreases from 15 M^{-1} at 8 °C to 5 M^{-1} at 45 °C. A van't Hoff plot of these data yields an approximately straight line with $\Delta H° = -2.15$ kcal/mol, consistent with the direct calorimetric measurement.

The effective peptide charge sensed at the membrane surface depends on the experimental conditions. For large unilamellar vesicles where the membrane surface is flat as compared to the dimensions of TAT-PTD, z_p reaches a maximum value of $z_p = +7$. Likewise, SUVs with a POPG content >40% require a large $z_p = +6$. For all other conditions, the effective charge was $z_p = +4$. As compared to the formal peptide charge of $z_p = +8$, it is obvious that not all charged groups can reach the membrane simultaneously. Optimum conditions are found for flat membranes or when the electrostatic attraction is particularly large.

The Gouy−Chapman theory can also explain apparent saturation behavior without resorting to Langmuir-type adsorption model (cf. Figure 4). If the peptide concentration is high enough as compared to the available lipid, an equilibrium is established between electrostatic attraction and dilution effects. For small K_p (i.e., small hydrophobic interactions), the membrane surface potential will be reduced to a critical limit ($\Psi_{crit} \approx -26$ mV for Figure 4) but will never be completely neutralized.

Binding of TAT-PTD Peptide to Membranes versus Binding to Heparan Sulfate. Using ITC, we have shown recently that TAT-PTD can bind tightly to glycosaminoglycans such as heparan sulfate, heparin, and chondroitin sulfate B (*42*). The binding to these linear, anionic macromolecules follows a multisite-binding model, formally identical to eq 5. However, now the glycosaminoglycan is the mulit-site template, M, and the peptide is the ligand, L. The binding constant of TAT-PTD to an individual binding site is $K_0 \sim 10^6$ M^{-1}, which is 2−3 orders of magnitude larger than the binding of TAT-PTD to the PG lipid. Binding of TAT-PTD peptides to glycosamino glycans on the outside of a biological cell membrane is thus thermodynamically and statistically more probable than binding to anionic phospholipids, in particular since the latter are mainly located on the cytosolic side of the membrane (*43*).

The TAT-PTD binding to lipid membranes as well as to glycosaminoglycans is an exothermic process. The measured $\Delta H°$ values are, however, less negative for lipids than for glycosaminoglycans. More importantly, $\Delta H°$ for lipid binding decreases with temperature leading to a small negative $\Delta C_p° = -13$ cal/(mol peptide K), which is in contrast to the positive $\Delta C_p° = +135$ cal/(mol K) found for the binding to heparan sulfate. A positive $\Delta C_p°$ is typical for a charge neutralization reaction, and a negative $\Delta C_p°$ is characteristic of a hydrophobic interaction where water molecules are released as two hydrophobic surfaces come into close contact. In the TAT-PTD membrane equilibrium, the two opposing forces appear to balance each other leading to $\Delta C_p°$ close to zero.

A weak hydrophobic interaction is further supported by the small hydrophobic partition constants of $K_p \sim 1-15$ M^{-1} (at all POPG concentrations). The corresponding free energies can be calculated according to $\Delta G° = -RT \ln(55.5\ K)$ where the factor 55.5 is the molar concentration of water. In the electrostatic attraction/chemical partition model, the concentration in the membrane phase is given in mole fraction units; the concentration in the aqueous phase, however, is given in mol/L. The factor 55.5 transforms the concentration in the aqueous phase into mole fractions and corrects for the entropic dilution effect (*44*). With this correction, Table 1 demonstrates that enthalpy and entropy contribute to equal extent to membrane binding at low temperatures and that the reaction is exclusively enthalpy-driven at high temperatures. This is again in contrast to TAT-PTD binding to heparan sulfate where the entropic term is dominant.

Comparison of TAT-PTD with other Polycationic Peptides. On the basis of the high charge density of TAT-PTD (eight out of 11 positively charged, $z_p = +8$), the peptide may be compared with the results obtained for polylysines. Murray et al. (*45*) have studied in detail the binding of heptalysine with and without attached fluorescence label to vesicles

formed from mixtures of the acidic lipids (phosphatidylserine (PS) or phosphatidylglycerol) and PC. For membranes composed of 5:1 PC/PS and 5:1 PC/PG, a binding constant of $K_0 \approx 6 \times 10^2$ M^{-1} was reported for unlabeled Lys_7 using the same model as eq 1. Taking into account the smaller charge of the heptalysine as well as that of the membranes employed, the binding constant reported by Murray et al. (*45*) is consistent with the K_0 value reported in Table 1.

Membrane binding data have recently been reported for another CPP, penetratin (RQIKIWFQNRRMKWKK, also called *pAntp*). It is a 16-residue fragment from the *Drosophila* transcription factor *Antennapedia*. Penetratin carries seven positive charges that are separated by hydrophobic residues. On the basis of studies with cell cultures, it has been concluded that penetratin—much like TAT-PTD—enters into cells by a receptor-independent internalization process (*46*−*50*). Again, the mechanism is unknown, but binding to the lipid part of the cell membrane has been implied (*51*). The binding isotherm of penetratin to charged lipid membranes has recently been investigated by two different groups taking advantage of the trp fluorescence of this peptide (*5*, *52*). The binding isotherms were analyzed either in terms of the uncorrected partition equilibrium (eq 9; ref *5*) or in terms of the electrostatic attraction/surface partition model (eq 7; ref *52*). In the first study (*5*) it was concluded "that pAntp remains on the outer leaflet ... and does not translocate through the phospholipid bilayer". The apparent binding constant was $K_{app} \sim 1.3 \times 10^4$ M^{-1}. In the second study (*52*), a rapid translocation of the peptide across the membrane was postulated based on earlier, indirect evidence (*51*). The intrinsic binding constant was deduced as $K_p \sim 80$ M^{-1}, the apparent binding constant was $K_{app} \sim 4.5 \times 10^6$ M^{-1}. The latter was thus distinctly higher than that of Drin et al. (*5*). Comparing these results with the TAT-PTD data presented in this study it is obvious that penetratin binds better than TAT-PTD to lipid membranes for two reasons: (i) the hydrophobic residues of penetratin can probably intercalate between the lipids and (ii) membrane binding of penetratin is accompanied by helix formation. The molecule becomes partially α-helical in micellar environment or when in contact with a charged lipid membrane. The helix content is ∼40% in SDS and ∼40−60% when penetratin is bound to PC/PG membranes (*5*, *52*). The latter process contributes a negative free energy of ∼0.14 kcal/mol per helix residue to binding (*53*). If 50% of penetratin forms an α-helix, this corresponds to a gain in free energy of about −1.1 kcal/mol, or to a factor of 6−7 in the binding constant. This corresponds to the difference in K_0 between TAT-PTD and penetratin. It should be noted that TAT-PTD does not undergo a conformational change under similar conditions. We have measured CD spectra of this peptide in buffer and in the presence of POPC/POPG (75:25 mol %) vesicles and observed a random-coil structure in both cases (spectra not shown) (see also ref *54*).

In conclusion, the binding of TAT-PTD to a negatively charged lipid membrane is initiated by a strong electrostatic interaction followed by some weak hydrophobic adsorption/partitioning. The total free energy of binding for TAT-PTD (at 1 μM equilibrium concentration) in equilibrium with lipid vesicles containing 25% anionic lipid is $\Delta G^\circ = -5.2$ kcal/mol and is composed of an electrostatic contribution $\Delta G_{el} = -RT \ln(C_M/C_{eq}) \approx -4.0$ kcal/mol and a hydrophobic contribution $\Delta G_h = -RT \ln K_p = -1.2$ kcal/mol. Thus, ∼77% of the free energy of binding is electrostatic in origin. A consistent interpretation of the binding isotherms obtained with four different experimental methods was only possible by assuming that TAT-PTD binds to the vesicle outside only. From the NMR data it further follows that TAT-PTD binding leaves the bilayer membrane intact. Under no condition could we detect a nonbilayer phase, and no dye leakage was induced by TAT-PTD from 100 nm vesicles (up to 50% POPG). HIV-1 TAT-PTD is only weakly surface active, and the Gibbs adsorption isotherm yields a rough estimate of a molecular area of ∼250 Å^2. A small part of this area, ∼100 Å^2, is in contact with the lipid bilayer as judged from film expansion studies. Finally, the addition of TAT-PTD to the lipid membrane does not induce domain formation. Neutral and anionic lipids remain mixed randomly. Nevertheless, there is a positional preference of TAT-PTD for anionic lipids as evidenced by the changes of the ^{2}H-NMR spectra of headgroup labeled POPG. The present studies argue against the translocation of TAT-PTD across a pure PG/PC lipid membrane. It is thus unlikely that anionic lipids alone play a major part in the translocation of TAT-PTD across biological membranes. The binding of TAT-PTD to glycosaminoglycans on the outer cell surface is distinctly more probable for thermodynamic and statistical reasons.

REFERENCES

1. Lindgren, M., Hallbrink, M., Prochiantz, A., and Langel, U. (2000) Cell-penetrating peptides, *Trends Pharmacol. Sci. 21*, 99−103.
2. Frankel, A. D., and Pabo, C. O. (1988) Cellular uptake of the tat protein from human immunodeficiency virus, *Cell 55*, 1189−93.
3. Green, M., and Loewenstein, P. M. (1988) Autonomous functional domains of chemically synthesized human immunodeficiency virus tat trans-activator protein, *Cell 55*, 1179−88.
4. Thorén, P. E., Persson, D., Karlsson, M., and Norden, B. (2000) The antennapedia peptide penetratin translocates across lipid bilayers—the first direct observation, *FEBS Lett. 482*, 265−8.
5. Drin, G., Demene, H., Temsamani, J., and Brasseur, R. (2001) Translocation of the pAntp peptide and its amphipathic analogue AP-2AL, *Biochemistry 40*, 1824−34.
6. Tyagi, M., Rusnati, M., Presta, M., and Giacca, M. (2001) Internalization of HIV-1 tat requires cell surface heparan sulfate proteoglycans, *J. Biol. Chem. 276*, 3254−61.
7. Prochiantz, A. (2000) Messenger proteins: homeoproteins, TAT, and others, *Curr. Opin. Cell Biol. 12*, 400−6.
8. von Heijne, G. (2000) Membrane permeability—Transport of peptides and proteins through membranes—Editorial overview, *Curr. Opin. Cell Biol. 12*, 399.
9. Gally, H. U., Niederberger, W., and Seelig, J. (1975) Conformation and motion of the choline headgroup in bilayers of dipalmitoyl-3-*sn*-phosphatidylcholine, *Biochemistry 14*, 3647−52.
10. Wohlgemuth, R., Waespe-Sarcevic, N., and Seelig, J. (1980) Bilayers of phosphatidylglycerol. A deuterium and phosphorus nuclear magnetic resonance study of the headgroup region, *Biochemistry 19*, 3315−21.
11. Buser, C. A., and McLaughlin, S. (1998) Ultracentrifugation technique for measuring the binding of peptides and proteins to sucrose-loaded phospholipid vesicles, *Methods Mol. Biol. 84*, 267−81.
12. Seelig, A., Alt, T., Lotz, S., and Holzemann, G. (1996) Binding of substance P agonists to lipid membranes and to the neurokinin-1 receptor, *Biochemistry 35*, 4365−74.
13. Seelig, A. (1987) Local anesthetics and pressure: a comparison of dibucaine binding to lipid monolayers and bilayers, *Biochim. Biophys. Acta 899*, 196−204.
14. Seelig, A. (1992) Interaction of a substance P agonist and of substance P antagonists with lipid membranes. A thermodynamic analysis, *Biochemistry 31*, 2897−904.
15. Boguslavsky, V., Rebecchi, M., Morris, A. J., Jhon, D. Y., Rhee, S. G., and McLaughlin, S. (1994) Effect of monolayer surface pressure on the activities of phosphoinositide-specific phospholipase C-β 1, -γ 1, and -δ 1, *Biochemistry 33*, 3032−7.

16. Wieprecht, T., Beyermann, M., and Seelig, J. (1999) Binding of antibacterial magainin peptides to electrically neutral membranes: thermodynamics and structure, *Biochemistry 38*, 10377−87.
17. van Holde, K. E., Johnson, W. C., and Ho, S. P. (1998) *Principles of Physical Biochemistry*, p 605, Prentice Hall, Upper Saddle River, New Jersey.
18. Seelig, J. (1997) Titration calorimetry of lipid−peptide interactions, *Biochim. Biophys. Acta 1331*, 103−16.
19. Wiseman, T., Williston, S., Brandts, J. F., and Lin, L. N. (1989) Rapid measurement of binding constants and heats of binding using a new titration calorimeter, *Anal. Biochem. 179*, 131−7.
20. Michaelson, D. M., Horwitz, A. F., and Klein, M. P. (1973) Transbilayer asymmetry and surface homogeneity of mixed phospholipids in cosonicated vesicles, *Biochemistry 12*, 2637−45.
21. Aveyard, R., and Haydon, D. A. (1973) *An introduction to the principles of surface chemistry*, Cambridge University Press, London.
22. McLaughlin, S. (1977) Electrostatic potentials at membrane−solution interfaces, *Curr. Top. Membr. Transp. 9*, 71−144.
23. Beschiaschvili, G., and Seelig, J. (1990) Peptide binding to lipid bilayers. Binding isotherms and ζ-potential of a cyclic somatostatin analogue, *Biochemistry 29*, 10995−1000.
24. Seelig, J., Nebel, S., Ganz, P., and Bruns, C. (1993) Electrostatic and nonpolar peptide−membrane interactions. Lipid binding and functional properties of somatostatin analogues of charge $z = +1$ to $z = +3$, *Biochemistry 32*, 9714−21.
25. Seelig, J. (1978) ^{31}P nuclear magnetic resonance and the headgroup structure of phospholipids in membranes, *Biochim. Biophys. Acta 515*, 105−40.
26. Seelig, J., Macdonald, P. M., and Scherer, P. G. (1987) Phospholipid headgroups as sensors of electric charge in membranes, *Biochemistry 26*, 7535−41.
27. Niederberger, W., and Seelig, J. (1974) Deuterium magnetische Resonanzspektroskopie an spezifisch deuterierten flüssigen Kristallen, *Ber. Bunsen-Ges. Physik. Chem. 78*, 947−9.
28. Macdonald, P. M., and Seelig, J. (1987) Calcium binding to mixed phosphatidylglycerol−phosphatidylcholine bilayers as studied by deuterium nuclear magnetic resonance, *Biochemistry 26*, 1231−40.
29. Akutsu, H., and Seelig, J. (1981) Interaction of metal ions with phosphatidylcholine bilayer membranes, *Biochemistry 20*, 7366−73.
30. Altenbach, C., and Seelig, J. (1984) Ca^{2+} binding to phosphatidylcholine bilayers as studied by deuterium magnetic resonance. Evidence for the formation of a Ca^{2+} complex with two phospholipid molecules, *Biochemistry 23*, 3913−20.
31. Seelig, A., Allegrini, P. R., and Seelig, J. (1988) Partitioning of local anesthetics into membranes: surface charge effects monitored by the phospholipid headgroup, *Biochim. Biophys. Acta 939*, 267−76.
32. Boulanger, Y., Schreier, S., and Smith, I. C. (1981) Molecular details of anesthetic−lipid interaction as seen by deuterium and phosphorus-31 nuclear magnetic resonance, *Biochemistry 20*, 6824−30.
33. Schote, U., and Seelig, J. (1998) Interaction of the neuronal marker dye FM1-43 with lipid membranes. Thermodynamics and lipid ordering, *Biochim. Biophys. Acta 1415*, 135−46.
34. Bäuerle, H. D., and Seelig, J. (1991) Interaction of charged and uncharged calcium channel antagonists with phospholipid membranes. Binding equilibrium, binding enthalpy, and membrane location, *Biochemistry 30*, 7203−11.
35. Thomas, P. G., and Seelig, J. (1993) Binding of the calcium antagonist flunarizine to phosphatidylcholine bilayers: charge effects and thermodynamics, *Biochem. J. 291*, 397−402.
36. Kuchinka, E., and Seelig, J. (1989) Interaction of melittin with phosphatidylcholine membranes. Binding isotherm and lipid headgroup conformation, *Biochemistry 28*, 4216−21.
37. Beschiaschvili, G., and Seelig, J. (1991) Peptide binding to lipid membranes. Spectroscopic studies on the insertion of a cyclic somatostatin analogue into phospholipid bilayers, *Biochim. Biophys. Acta 1061*, 78−84.
38. Spuhler, P., Anantharamaiah, G. M., Segrest, J. P., and Seelig, J. (1994) Binding of apolipoprotein A-I model peptides to lipid bilayers. Measurement of binding isotherms and peptide−lipid headgroup interactions, *J. Biol. Chem. 269*, 23904−10.
39. Roux, M., Neumann, J. M., Bloom, M., and Devaux, P. F. (1988) ^{2}H and ^{31}P NMR study of pentalysine interaction with headgroup deuterated phosphatidylcholine and phosphatidylserine, *Eur. Biophys. J. 16*, 267−73.
40. Franzin, C. M., and Macdonald, P. M. (2001) Polylysine-induced H-2 NMR-observable domains in phosphatidylserine/phosphatidylcholine lipid bilayers, *Biophys. J. 81*, 3346−62.
41. May, S., Harries, D., and Ben-Shaul, A. (2000) Lipid demixing and protein−protein interactions in the adsorption of charged proteins on mixed membranes, *Biophys. J. 79*, 1747−60.
42. Ziegler, A., and Seelig, J. Interaction of protein transduction domain of HIV-1 TAT with heparan sulfate. Binding mechanism and thermodynamic parameters, submitted.
43. Bratton, D. L., Fadok, V. A., Richter, D. A., Kailey, J. M., Guthrie, L. A., and Henson, P. M. (1997) Appearance of phosphatidylserine on apoptotic cells requires calcium-mediated nonspecific flip-flop and is enhanced by loss of the aminophospholipid translocase, *J. Biol. Chem. 272*, 26159−65.
44. Cantor, C. R., and Schimmel, P. R. (1980) *Biophysical Chemistry*, Vol. 1, p 283 Freeman, San Francisco.
45. Murray, D., Arbuzova, A., Hangyas-Mihalyne, G., Gambhir, A., Ben-Tal, N., Honig, B., and McLaughlin, S. (1999) Electrostatic properties of membranes containing acidic lipids and adsorbed basic peptides: theory and experiment, *Biophys. J. 77*, 3176−88.
46. Derossi, D., Joliot, A. H., Chassaing, G., and Prochiantz, A. (1994) The third helix of the *Antennapedia* homeodomain translocates through biological membranes, *J. Biol. Chem. 269*, 10444−50.
47. Scheller, A., Oehlke, J., Wiesner, B., Dathe, M., Krause, E., Beyermann, M., Melzig, M., and Bienert, M. (1999) Structural requirements for cellular uptake of α-helical amphipathic peptides, *J. Pept. Sci. 5*, 185−94.
48. Derossi, D., Calvet, S., Trembleau, A., Brunissen, A., Chassaing, G., and Prochiantz, A. (1996) Cell internalization of the third helix of the *Antennapedia* homeodomain is receptor-independent, *J. Biol. Chem. 271*, 18188−93.
49. Brugidou, J., Legrand, C., Mery, J., and Rabie, A. (1995) The retro-inverso form of a homeobox-derived short peptide is rapidly internalized by cultured neurones: a new basis for an efficient intracellular delivery system, *Biochem. Biophys. Res. Commun. 214*, 685−93.
50. Fischer, P. M., Zhelev, N. Z., Wang, S., Melville, J. E., Fahraeus, R., and Lane, D. P. (2000) Structure−activity relationship of truncated and substituted analogues of the intracellular delivery vector Penetratin, *J. Pept. Res. 55*, 163−72.
51. Thoren, P. E., Persson, D., Karlsson, M., and Norden, B. (2000) The antennapedia peptide penetratin translocates across lipid bilayers—the first direct observation, *FEBS Lett 482*, 265−8.
52. Persson, D., Thoren, P. E., Herner, M., Lincoln, P., and Norden, B. (2003) Application of a novel analysis to measure the binding of the membrane-translocating peptide penetratin to negatively charged liposomes, *Biochemistry 42*, 421−9.
53. Wieprecht, T., Apostolov, O., Beyermann, M., and Seelig, J. (1999) Thermodynamics of the α-helix−coil transition of amphipathic peptides in a membrane environment: implications for the peptide−membrane binding equilibrium, *J. Mol. Biol. 294*, 785−94.
54. Mitchell, D. J., Kim, D. T., Steinman, L., Fathman, C. G., and Rothbard, J. B. (2000) Polyarginine enters cells more efficiently than other polycationic homopolymers, *J. Pept. Res. 56*, 318−25.

BI0346805